Dynamics of the O + CN Reaction and N + CO Scattering on Two Coupled Surfaces[†]

Erik Abrahamsson,[‡] Stefan Andersson,[‡] Nikola Marković,[§] and Gunnar Nyman*[,‡]

Department of Chemistry, Physical Chemistry, University of Gothenburg, SE-412 96 Gothenburg, Sweden, and Department of Chemical and Biological Engineering, Physical Chemistry, Chalmers, University of Technology, SE-412 96 Gothenburg, Sweden

Received: May 27, 2009; Revised Manuscript Received: September 9, 2009

Spin−orbit coupling between the two collinear $^2\Pi$ and $^4\Sigma^-$ potential energy surfaces for the NCO system are calculated using the RASSI method with CASSCF wave functions as basis set. The GDVR method has been used to interpolate a spin−orbit coupling surface.

Wave packet and quasi-classical trajectory surface hopping calculations have been performed and compared for both the $O(^3P) + CN(X^2\Sigma^+) \rightarrow N(^4S) + CO(X^1\Sigma^+)$ reaction and for electronically inelastic scattering in the N + CO channels.

The O + CN nonadiabatic reaction probabilities are small. The wavepacket study gives a resonance structure. Also for the N + CO electronically inelastic scattering the wave packet calculations give a distinct resonance structure with peak transition probabilities up to around 10%, which is somewhat lower than the trajectory surface hopping results.

Introduction

The triatomic system consisting of the C, N, and O atoms has been the subject of numerous studies, both theoretical and experimental. The system is of interest in such diverse areas of science as combustion[1] and astrophysics.[2−5]

In this study the dynamics of the reaction of ground state oxygen atoms with cyanogen radicals

$$O(^3P) + CN(X^2\Sigma^+) \rightarrow N(^2D) + CO(X^1\Sigma^+) \qquad (1)$$

and

$$O(^3P) + CN(X^2\Sigma^+) \rightarrow N(^4S) + CO(X^1\Sigma^+) \qquad (2)$$

with spin−orbit coupling between the electronic states is investigated. It is believed that the O + CN reaction is one of the most important sources of CN destruction both in combustion and in interstellar clouds. The cyanogen radical is of interest in astrophysics as it is thought to be an important precursor to more complex molecules, such as cyanopolyynes, $HC_{2n+1}N$.[3,4,6] Kinetic modeling of interstellar chemistry is therefore quite sensitive to the rate of the O + CN reaction.[4]

Detailed studies of reactions 1 and 2 were performed in the 1970s by Schmatjko and Wolfrum.[7,8] They performed both quasi-classical trajectory (QCT) calculations on empirical London−Eyring−Polanyi−Sato (LEPS) type potential energy surfaces and experimental investigations of the dynamics and kinetics of reactions 1 and 2. From their room temperature experiments they concluded that about 20% of the reactive events produced $CO(X^1\Sigma^+) + N(^4S)$, corresponding to reaction 2 above.

Electronic potential energy surfaces of different multiplicity may cross each other. At these crossings, spin−orbit coupling can allow transitions between the potential energy surfaces. Such crossings can thus affect the dynamics of a molecular system, allowing spin-forbidden transitions and bypassing of potential barriers. The two lowest collinear potential energy surfaces $^2\Pi$ and $^4\Sigma^-$ of the OCN system, corresponding to reactions 1 and 2, respectively, have previously been calculated.[9]

In the ground state, NCO is a linear molecule,[9−11] and the long-range attraction between O and CN is the strongest in the collinear configuration.[12] With this in mind, using the collinear approach for the dynamics of reaction 1 can be motivated. Recent CASPT2 calculations on the lowest $^4A''$ surface ($^4\Sigma^-$ in $C_{\infty v}$ symmetry), however, indicate that the collinear configuration might not be important for the *adiabatic* single-surface mechanism of reaction 2.[13] Little is known about the importance of spin−orbit induced nonadiabatic transitions between the lowest doublet and quartet surfaces in this system. These could potentially be an important component of the rate of reaction 2, in addition to the adiabatic reaction pathway. Wave packet dynamics with spin−orbit coupled surfaces for reactions with heavy elements have also not previously been reported, and the system makes an interesting model study.

This study will investigate the effects of spin−orbit coupling on the reaction probabilities for the two reactions in collinear configuration. We first present the spin−orbit elements for the electronic states for reactions 1 and 2, based on ab initio calculations. Thereafter two sets of time-dependent dynamic calculations with spin−orbit coupling are reported. The first dynamic calculations are based on the reaction O + CN → N + CO, i.e., reactions 1 and 2, with coupled electronic states. The second set of calculations are studies of the relaxation of nitrogen, from the excited $N(^2D)$ to the ground state $N(^4S)$, via the NCO complex, on the two surfaces.

Computational Details

Potential Energy Surfaces. The potential energy surfaces used in this study were calculated and used in our previous study

[†] Part of the "Vincenzo Aquilanti Festschrift".

* To whom correspondence should be addressed, nyman@chem.gu.se.
[‡] University of Gothenburg.
[§] Chalmers University of Technology.

10.1021/jp904954k
Published on Web 10/07/2009

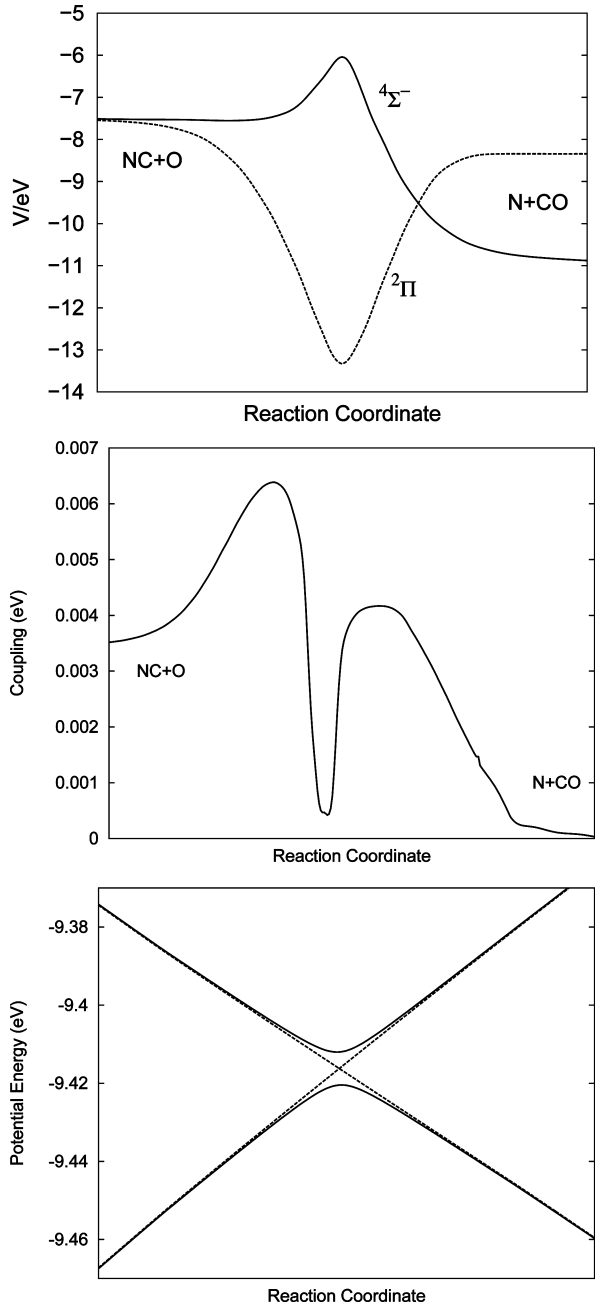

Figure 1. Minimum energy paths connecting O + CN and N + CO for the $^2\Pi$ and $^4\Sigma^-$ surfaces (top). Spin−orbit coupling along the minimum energy path of the $^2\Pi$ surface (center). Detail of the diabatic and adiabatic surfaces at the crossing along the minimum energy path of the $^2\Pi$ surface (bottom). Note that in the upper panel (identical to Figure 2 of ref 9) each surface has its own reaction coordinate whereby the energy of the crossing point must not be read from the graph.

of the dynamics of the O + CN system.[9] The lowest collinear $^2\Pi$ and $^4\Sigma^-$ states were calculated at the CASPT2 level of theory, using MOLCAS 5.2,[14] as described in detail in ref 9.

The generalized discrete variable representation (GDVR) method[15,16] was used to interpolate a smooth potential energy surface using 484 energy points for each symmetry. Of the 484 energy points used for the interpolation, 171 were calculated using CASPT2 in the atom−atom separation range 0.83−12.97 Å (see ref 9 for details).

In Figure 1 the minimum energy path on the two surfaces is shown. Both reactions are exothermic, with an energy difference of 0.81 eV for the $^2\Pi$ surface and 3.39 eV for the $^4\Sigma^-$ surface.

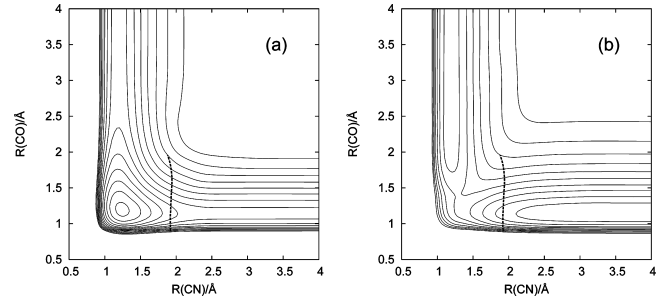

Figure 2. Illustration of the $^2\Pi$ (a) and $^4\Sigma^-$ (b) potential energy surfaces. The dashed lines indicate where the two surfaces cross each other.

The $^2\Pi$ surface has a 5.85 eV deep potential well, while the $^4\Sigma^-$ surface has a potential energy barrier of 1.42 eV. It is thus only on the $^2\Pi$ surface that reaction is thermally accessible at room temperature. The surfaces are further illustrated in Figure 2 where the crossing between the surfaces is also indicated.

We note here that a complete picture of the asymptotic fine-structure (spin−orbit) states should include not only the $^4\Sigma^-$ and $^2\Pi$ states but also a $^2\Sigma^-$ and a $^4\Pi$ state. In regions where the intermolecular interaction become much larger than the spin−orbit energy splitting, the dynamics will be dominated by either, or both, of the first two electronic states.

Spin−Orbit Coupling Elements. The spin−orbit interaction matrix elements were calculated using the MOLCAS 6.0 program package.[17] We used the RASSI (restricted active space state interaction) method to calculate the spin−orbit couplings, using wave functions obtained from CASSCF calculations as basis set. As for the potential energy points, an ANO-L basis set with the 14s9p4d3f primitive set contracted to 4s3p2d1f was used.

Twice the number of points in each coordinate was used to calculate the spin−orbit surface, compared to the calculations of the potential energy surfaces. The resulting spin−orbit coupling surface has more rapid changes and more complicated shape than the PES, demanding a greater number of points to accurately represent the surface using GDVR; 684 CASSCF/RASSI points were calculated with an atom−atom distance in the range from 0.83 to 4.67 Å in each coordinate (R_{CO} and R_{CN}). The points were evenly distributed in the coordinate $x_i = \ln R_i$ ($R_i = R_{CO}$ or R_{CN}), resulting in a more detailed description of the reaction zone. No calculations were made in the region where both coordinates are greater than 2.47 Å.

Quantum Scattering Calculations. The Schrödinger equation for the system consisting of two coupled electronic states (here denoted Σ and Π) can be written as

$$i\hbar\frac{\partial}{\partial t}\begin{pmatrix}\Psi_\Pi\\ \Psi_\Sigma\end{pmatrix} = \left[\begin{pmatrix}\hat{T} & 0\\ 0 & \hat{T}\end{pmatrix} + \begin{pmatrix}V_1 & V_{12}\\ V_{12}^* & V_2\end{pmatrix}\right]\begin{pmatrix}\Psi_\Pi\\ \Psi_\Sigma\end{pmatrix} \quad (3)$$

where V_1 and V_2 are the diabatic potential terms and V_{12} is the coupling term. $\hat{T}$ is the nuclear kinetic energy operator. The wave packet is propagated by solving the time-dependent Schrödinger equation using the split-operator[18] method. In order to solve eq 3, the potential energy matrix has to be diagonalized by the unitary transformation

$$\mathbf{D} = \mathbf{U}^\dagger\mathbf{V}\mathbf{U} \quad (4)$$

where **D** is diagonal. Then the exponent of the matrix **V** can be written as

$$e^{\mathbf{V}} = \mathbf{U}e^{\mathbf{D}}\mathbf{U}^{\dagger} \tag{5}$$

and the split-operator method can be used to propagate the wave packet on the two coupled electronic surfaces.

The time-dependent wave packet propagations were carried out using mass-weighted product Jacobi coordinates ($\tilde{R}$,$\tilde{r}$), the product being the CO diatom and the N atom, as in our previous work.[9] The wave packet was initialized on either of the two adiabatic surfaces as a linear superposition of components on the two diabatic surfaces. For initiation on the lower adiabatic surface we set

$$\Psi = \frac{1}{\sqrt{2}}(-i, 1)\begin{pmatrix}\Psi_{\Pi}\\ \Psi_{\Sigma}\end{pmatrix} \tag{6}$$

and for initiation on the upper adiabat we set

$$\Psi = \frac{1}{\sqrt{2}}(-i, -1)\begin{pmatrix}\Psi_{\Pi}\\ \Psi_{\Sigma}\end{pmatrix} \tag{7}$$

The component on each of the diabatic surfaces was constructed as a product of a vibrational eigenstate of the diatom and a translational function in the form of a Gaussian wave packet with the same parameters on both diabats. The wave packet propagations were carried out for grid sizes {0.5, 22} Å and {0.5, 18} Å in product Jacobi coordinates, r and R, respectively, using 1680 grid points or more in each coordinate. The time step was 0.1 fs, and the propagations were continued until more than 99.995% of the wave packet had left the grid. The initial wave packet was centered at an R distance of 15 Å, where the two diabats are flat. Convergence tests of the parameters have been made. The outgoing wave packet was analyzed in an energy interval corresponding to 97.5% of the energy distribution in the incident Gaussian.

Reflection of the wave packet from the grid boundary is avoided by applying an exponential damping function suggested by Vibók and Balint-Kurti.[19] A time-dependent scale factor in the exponential damping function was employed as the average product kinetic energy substantially decreases with time. Different damping parameters have to be used for the two diabatic surfaces, as the kinetic energies on them are quite different in the product arrangement.

The scattered wave packet was projected onto asymptotic vibrational eigenstates at the projection point $R = R_p$ on both surfaces.

The time-dependent amplitudes are Fourier transformed to energy space, and the state-to-state reaction probabilities are calculated as the ratio between the scattered and the incident fluxes.[9,20]

Quasi-Classical Trajectories with Surface Hopping. The trajectory surface hopping (TSH) methodology used is based on the formulation given by Stine and Muckerman,[21] where the trajectories are propagated on the adiabatic surfaces. The internal state of the molecule is selected quasi-classically, and the equations of motion are integrated using the Gauss−Radau integrator.[22,23] At every step during the integration the Massey parameter, ω_{ij}, is evaluated[21,24,25]

$$\omega_{ij} = |(E_i - E_j)/(\mathbf{v}_i \cdot \langle\phi_i|\nabla\phi_j\rangle\hbar)| \tag{8}$$

where $\mathbf{v}_i$ is the nuclear velocity vector on adiabatic surface i and E_i, $i = 1, 2$, are the two eigenvalues of the potential matrix, i.e., the potential energies corresponding the two adiabatic electronic states, ϕ_i. Near an avoided crossing the matrix elements can be approximated as[24]

$$\left\langle \phi_i \frac{\partial \phi_j}{\partial q_k} \right\rangle = (E_j - E_i)^{-1}\mathbf{t}_i^{T}\frac{\partial \mathbf{V}}{\partial q_k}\mathbf{t}_j \tag{9}$$

where $\mathbf{t}_i$ are the eigenvectors obtained when diagonalizing the diabatic potential matrix, $\mathbf{V}$. If ω_{ij} has a minimum and if $\omega_{ij} < 1$ (or some other small number) the system may undergo a nonadiabatic transition. If a generated random number $\xi \in (0, 1)$ is less than the Landau−Zener probability, P_{LZ}[21]

$$P_{LZ} = \exp(-2\pi\gamma/\hbar) \tag{10}$$

where

$$\gamma = a^2/|(dW/dt)| \tag{11}$$

$$a = (E_1 - E_2)/2 \tag{12}$$

$$(dW/dt) = \sum_k (\partial \Delta W/\partial q_k) \cdot \dot{q}_k = \mathbf{n}\mathbf{M}^{-1}\mathbf{p}^{(2)} \tag{13}$$

a transition takes place. To evaluate the time rate of change of the difference in diabatic energies, $W = V_2 - V_1$, we first compute the matrix elements[21,24]

$$\beta_{km} = (4/2a)\mathbf{t}_2^{T}\frac{\partial \mathbf{V}}{\partial q_k}\mathbf{t}_1\mathbf{t}_2^{T}\frac{\partial \mathbf{V}}{\partial q_m}\mathbf{t}_1 \tag{14}$$

The matrix has only one nonzero eigenvalue and the corresponding eigenvector defines the unique direction along which the surface intersection behaves as a one-dimensional curve crossing. It turns out that this vector is given by any nontrivial row of the β-matrix, e.g., $(\beta_{11}, \beta_{12}, ..., \beta_{1n})$. The vector $\mathbf{n}$ is given by[21]

$$\mathbf{n} = (2a/\beta_{11})^{1/2}(\beta_{11}, \beta_{12}, ..., \beta_{1n}) \tag{15}$$

The momentum vector, $\mathbf{p}^{(2)}$, in eq 13 is given by[21]

$$\mathbf{p}^{(2)} = \mathbf{p}^{(1)} - \mathbf{n}\frac{\mathbf{n}\mathbf{M}^{-1}\mathbf{p}^{(1)}}{\mathbf{n}\mathbf{M}^{-1}\mathbf{n}}\left[1 - \left(1 - 2\Delta E\frac{\mathbf{n}\mathbf{M}^{-1}\mathbf{n}}{(\mathbf{n}\mathbf{M}^{-1}\mathbf{p}^{(1)})^2}\right)^{1/2}\right] \tag{16}$$

where ΔE is evaluated at the diabatic intersection, i.e., $\Delta E = \pm a$ and where $\mathbf{M}$ is the diagonal mass matrix. Finally, the momenta are modified after the transition using eq 16 with $\Delta E = E_f - E_i$ in order to conserve the total energy and the total angular momentum of the system. Our implementation of the trajectory surface hopping method has been tested by repeating some of the cross section calculations for $D^+ + H_2$ published by Schlier and co-workers[26] which are carried out using a slightly different technique. Despite the differences, the agreement between our test calculations and Schlier's results is good.

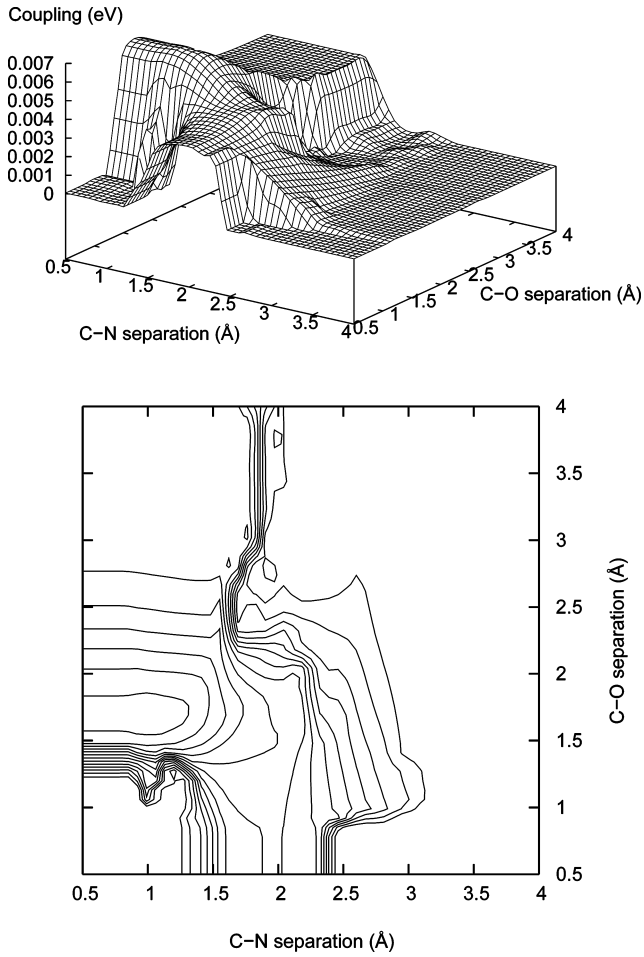

Figure 3. 3D view and contour plot of the spin−orbit coupling elements between the $^2\Pi$ and $^4\Sigma^-$ states. The spacing between the contours is 0.0005 eV.

Results

Spin−Orbit Coupling Elements. Figure 3 shows a 3D view and a contour plot of the CASSCF/RASSI spin−orbit coupling elements. As can be seen, the coupling is relatively strong in the asymptotic O + CN region, where the two electronic potential energy surfaces are degenerate or near-degenerate. The coupling is the strongest just before the reaction zone and goes through some twists and turns before finally dropping to zero in the asymptotic N + CO region. The shape of the spin−orbit surface along the minimum energy path of the $^2\Pi$ potential energy surface is shown in Figure 1. The crossing of the $^2\Pi$ and $^4\Sigma^-$ surfaces is located after the maximum, as seen in Figure 1. The adiabatic potential energy surfaces resulting from the spin−orbit coupling elements at the crossing between the two diabatic surfaces, along the minimum energy path, is also shown in Figure 1

The spin−orbit surface shown in Figure 3 has been modified before the GDVR interpolation, in order to produce a smooth surface. One prominent feature of the surface was a sharp ridge along $R_{CN} \approx 2.1$ Å. This ridge is outside the reaction channel, where the potential energies of the two surfaces are large and nearly degenerate. The wave packet never reaches this area, and to create a smoother and more "well-behaved" surface, this ridge was removed by linear interpolation in the R_{CN} direction. There were also two deep "holes" in the spin−orbit surface at $R_{CN} \approx$ 1.0 Å, $R_{CO} \approx 2.8$ Å, and at $R_{CN} \approx 1.5$ Å, $R_{CO} \approx 3.0$ Å, where the CASSCF/RASSI calculations would not converge. Calculations were made for several points around and close to these two '"problematic" geometries, and the values at the sought points were calculated using linear interpolation.

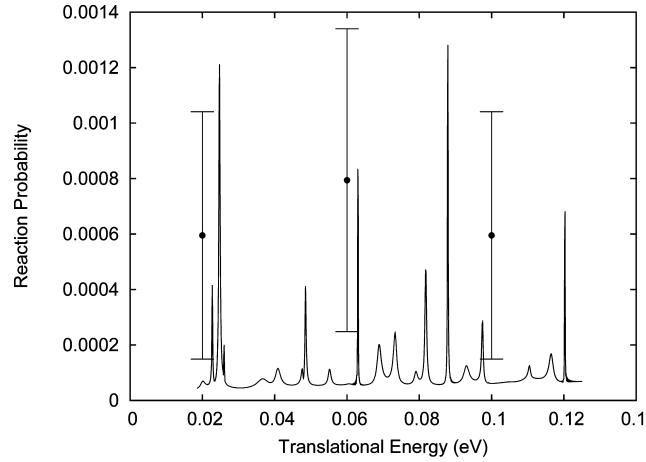

Figure 4. Probability for the reaction O + CN → N(^{4}S) + CO. The solid line represents wave packet probabilities and the dots trajectory surface hopping results, in both cases with initiation on the lower adiabat.

Scattering Calculations for the O + CN Channel. In the present work the wavepacket is initiated either on the lower or on the upper O + CN adiabat, rather than on the diabatic ($^2\Pi$ and $^4\Sigma^-$) surfaces as in our previous work.[9] In Figure 4 we show probabilities for ending up in the N(^{4}S) + CO electronic arrangement after initiation on the lower adiabat in the O + CN arrangement. The probabilities for this are small, even at the resonance positions. Trajectory surface hopping results are included for three translational energies. The statistical uncertainties in the TSH results are large. Still, it appears that the TSH probabilities are of the same order as the wave packet resonance peaks but clearly above the wave packet background probabilities. Overall, both the TSH and wave packet results indicate small reaction probabilities.

In our previous work,[9] where the coupling between the $^2\Pi$ and $^4\Sigma^-$ surfaces was neglected, it was found that the O + CN reaction on the $^2\Pi$ surface is direct and very fast, even though some slow components of the wave packet remain in the deep potential well for a long time. This is also reflected in the dynamics on the coupled surfaces. The wave packet will only be in the crossing region between the electronic surfaces a very short time, with a relatively high kinetic energy. This, together with the fact that the adiabatic surfaces bend sharply at the intersection (see Figure 1), makes the probability of the transition from the $^2\Pi$ to the $^4\Sigma^-$ surface very small.

In Figure 5 wave packet probabilities for coming out on the $^4\Sigma^-$ surface are shown for initiation on both the lower and the upper adiabats. At the energies shown, reaction on the $^4\Sigma^-$ surface does not occur, as a result of the high activation barrier. Formation of N(^{4}S) + CO can thus only occur as a result of the spin−orbit coupling between the two diabatic surfaces close to their intersection. For initiation on both the upper and the lower adiabat, the probability to transfer from the $^2\Pi$ to the $^4\Sigma^-$ surface around their intersection is small, even at the resonance peaks. It is seen that the resonance peaks occur at the same total energy (measured from a common zero level). We further note that the transfer probabilities are roughly a factor 4 larger when the initiation is on the upper adiabat. This relates to the details of the potential energy surfaces in the entrance channel (including coupling elements) as explained next.

Asymptotically in the reactant channel the adiabatic surfaces are completely flat (being adiabatic they are also uncoupled).

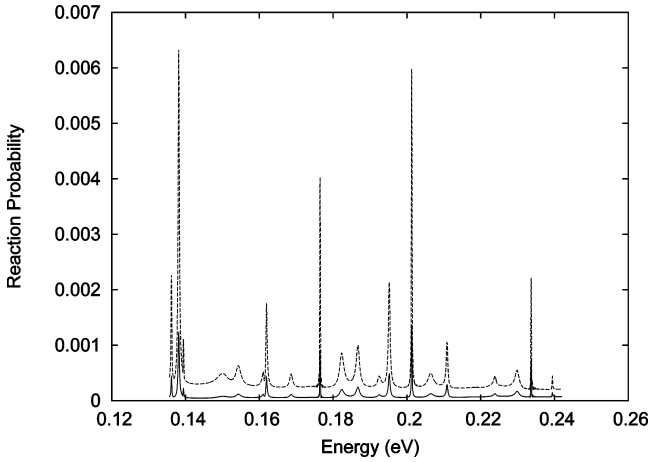

Figure 5. Probability for the reaction O + CN → N(^{4}S) + CO. The solid line represents initiation on the lower adiabat and the dashed line initiation on the upper adiabat.

In this region there is no transfer of the wave packet from the lower adiabat to the upper, or vice versa (note that there is transfer of the wave packet between the diabats). As the reactants approach each other, the wavepacket will begin to transfer between the adiabats as they begin to diverge, which can result from changes in the diabatic energies and from onset of variation in the coupling elements between the diabats. This means that even if the wave packet is initially on the lower adiabat, by the time it has moved to the interaction region, a fraction of it may now be on the upper surface. That fraction will be reflected by the high barrier on the $^4\Sigma^-$ surface. Similarly, if the wave packet is initiated on the upper adiabat, it may partially have transferred to the lower surface by the time it has reached the interaction region.

We have found that when the wave packet is initiated on the lower adiabat, roughly 80% of it is reflected by the barrier on the upper surface, meaning that this fraction had transferred to the upper surface by the time the interaction region was reached. When the wave packet is initiated on the upper surface, roughly 20% is reflected back. This means that the fraction of the wave packet reaching the region where the diabats cross is about 20% if initiated on the lower adiabat and about 80% if initiated on the upper adiabat. This largely explains the observed differences in probabilities seen in Figure 5.

We have noticed that in the TSH calculations there are hardly any transitions between the lower and upper adiabats before the avoided crossing is reached. Thus in Figure 4, while ~80% of the wave packet is reflected by the barrier on the upper surface, virtually no such reflection occurs in the TSH calculations. On the basis of this one would argue that the TSH probabilities should be roughly a factor 5 larger than the wave packet probabilities.

Compared to our previous study on the uncoupled surfaces[9] the present results are completely different. In the uncoupled case initiation on the upper adiabat yields no reaction at all in the energy range studied due to reflection in the barrier on that surface, while inititation on the lower adiabat yields essentially 100% reactivity (O + CN → N + CO). As explained above, when the surfaces are coupled, initiation on the upper adiabat yields higher reactivity than initiation on the lower adiabat due to transfer between the adiabats. At low temperature where the population on the two adiabats changes with temperature, this will affect the temperature dependence of the thermal rate constant.

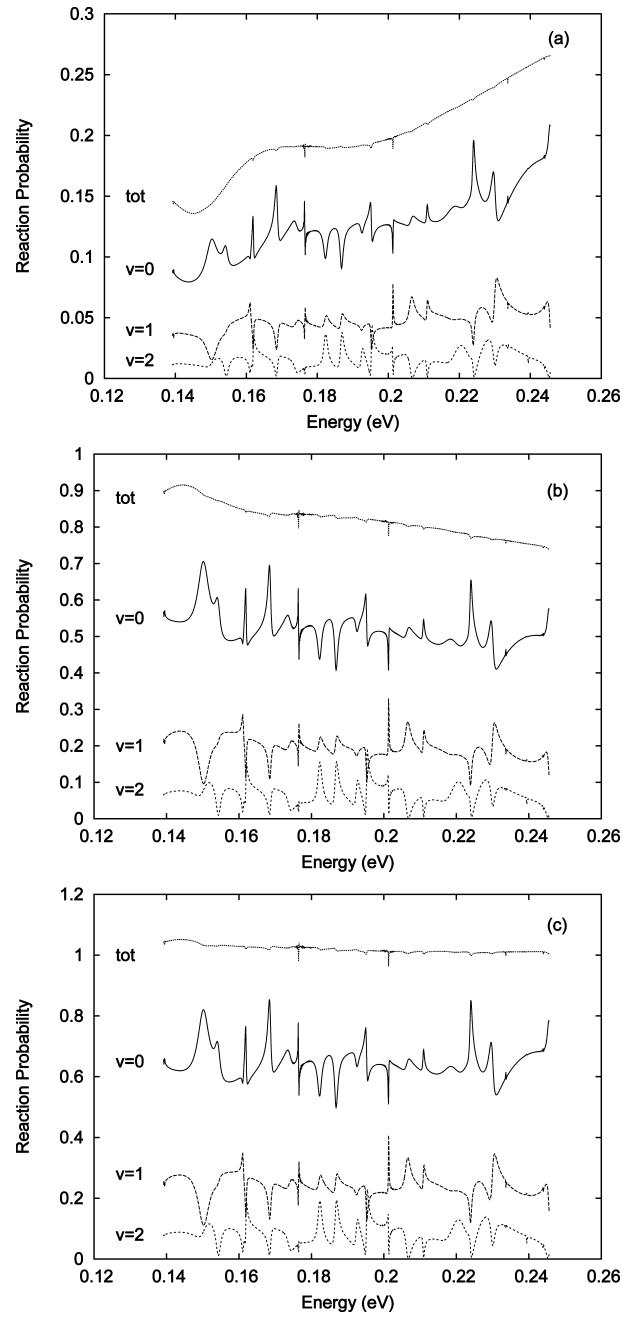

Figure 6. Probability as a function of energy for the reaction O + CN → N(^{2}D) + CO out of the ground vibrational state resolved on product vibrational states. Panel (a) represents initiation on the lower adiabat, (b) initiation on the upper adiabat, and (c) is the sum of the result for the lower and the upper adiabat. The energy is referenced to the asymptotic level of the diabats.

An interesting illustration of similarities between the present and previous results is shown in Figure 6 where reaction probabilities for reaction out of the initial vibrational ground state are resolved on different product vibrational states for initiation on the lower adiabat, the upper adiabat, and summed over the two. This figure can be compared with Figure 4 of ref 9. Note the similarity in the structure of the reaction probability between the figures.

Scattering Calculations for the N + CO Channel. Wave packet calculations were made for N + CO, starting in the N(^{2}D) + CO($X^1\Sigma^+$) state, with energies low enough not to allow for reactive processes. The wave packet can then only scatter elastically or inelastically, i.e., vibrationally and/or electronically.

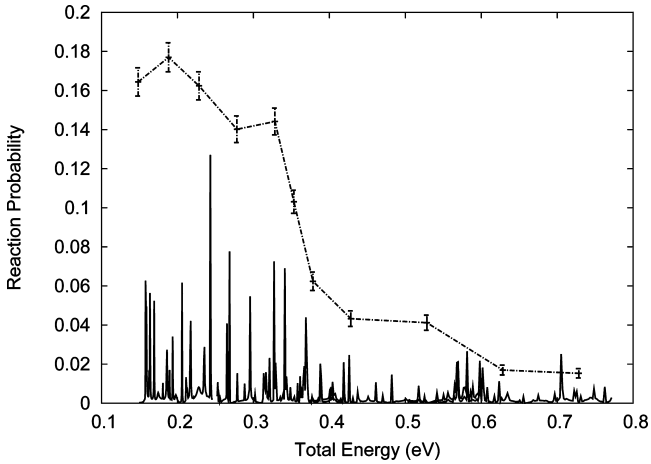

Figure 7. Total transition probability from the $^2\Pi$ surface to the $^4\Sigma^-$ surface for the process $N(^2D) + CO \rightarrow N(^4S) + CO$. Solid line represents quantum mechanical results. Dashed line represents quasi-classical results.

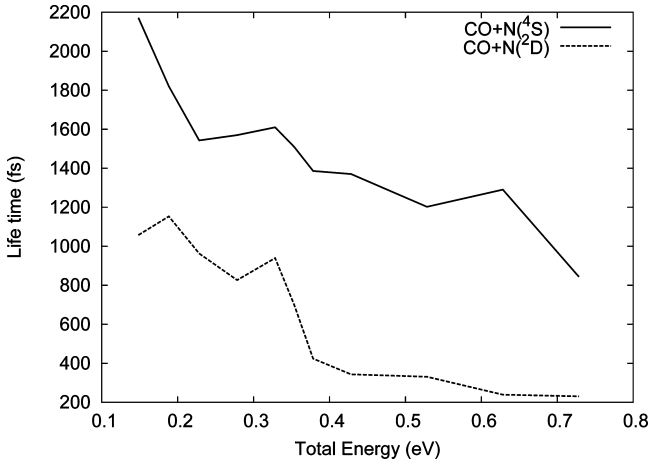

Figure 8. Average lifetimes of the complexes forming ground-state nitrogen (solid line) and excited nitrogen (dotted line) for scattering in the N + CO channel starting as $N(^2D)$ + CO.

The latter process involves crossing between the electronic potential energy surfaces to form ground-state nitrogen

$$N(^2D) + CO(X^1\Sigma^+) \rightarrow N(^4S) + CO(X^1\Sigma^+) \quad (17)$$

In this arrangement channel there is no asymptotic spin−orbit coupling, and the $^2\Pi$ potential energy surface is strongly attractive, without barriers.

In Figure 7 the transition probability from the $^2\Pi$ to the $^4\Sigma^-$ surface in the N + CO channel is shown. The wave packet calculations result in an average transition probability of about 0.5%, a result that differs greatly from the quasi-classical result. However, the wave packet results show a large number of resonance peaks throughout the energy interval, peaks that show the same general trend as the classical results—higher transition probability with lowered kinetic energy.

In the classical case, this can be understood in terms of speed, time, and passes over the crossing region. Figure 8 shows the lifetime of the complex, defined as the time from the first internuclear minimum distance exchange until the last,[27] for the trajectories exiting on the upper adiabatic surface (dotted line) and the trajectories exiting on the lower adiabatic surface, forming ground-state nitrogen (solid line). Comparing Figure 8 with Figure 7, we see that both the lifetime of the trajectories exiting on the upper adiabatic surface and the probability of a trajectory exiting on the lower adiabatic surface change quickly between 0.3 and 0.4 eV. Thus, we see a clear relation between the lifetime of the complex and the transition probability in the classical case. The longer the lifetime of the complex, the more passes over the crossing region and the larger the transition probability.

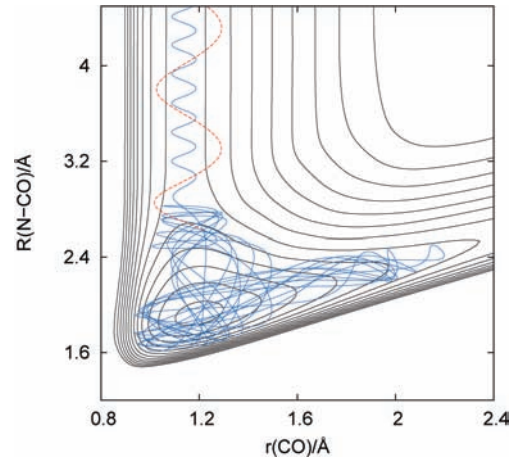

Figure 9. A trajectory initially on the $^2\Pi$ surface (solid line) which exits on the $^4\Sigma^-$ surface (dotted line) in the process $N(^2D) + CO \rightarrow N(^4S) + CO$.

Figure 9 shows a trajectory initiated in the $N(^2D) + CO(X^1\Sigma^+)$ channel on the $^2\Pi$ surface, with a total energy of 0.17 eV and initially in the vibrational ground state, plotted on the $^2\Pi$ surface. The trajectory makes in total 13 jumps between the surfaces and is drawn with a solid line until it makes the final jump onto the $^4\Sigma^-$ surface, where it is drawn with a dotted line.

Summary and Conclusions. We have calculated spin−orbit coupling elements between the lowest $^2\Pi$ and $^4\Sigma^-$ electronic states for the O + CN → N + CO reaction in collinear geometries. The spin−orbit coupling elements were obtained from CASSCF/RASSI electronic structure calculations, and interpolated by the GDVR method.[15] The $^2\Pi$ and $^4\Sigma^-$ electronic potential energy surfaces themselves were calculated at the CASPT2 level and have previously been reported in ref 9.

Wave packet calculations using the split operator method and trajectory surface hopping calculations have been performed. Calculations were performed with initiation in both the $O(^3P) + CN(X^2\Sigma^+)$ and the $N(^2D) + CO(X^1\Sigma^+)$ channels. In the first case, the kinetic energies studied were substantially lower than the potential energy barrier of the $^4\Sigma^-$ surface. A very small fraction reacting wave packet crossed over to the $^4\Sigma^-$ surface due to the spin−orbit interaction at the crossing. The TSH results are in overall agreement with the wave packet calculations.

For the $N(^2D) + CO(X^1\Sigma^+)$ channel the TSH calculations show a strong energy dependence in the transition probabilities to form $N(^4S) + CO(X^1\Sigma^+)$. For energies below approximately 0.35 eV, the probability of crossing over to the lower diabatic surface, producing ground state nitrogen, is over 15%, while higher energies only allow the creation of a few percent ground-state nitrogen. The wave packet calculations give small transition probabilities but with a distinct resonance pattern, with peaks reaching a transition probability of around 10%. The peaks are larger at lower energies. The TSH calculations are consistent with this trend. Even though the potential energy surface for approach of N to CO is collinearly dominated, the results may clearly change in a full-dimensional study.

Our results do not explain the 20% N(^{4}S) produced by crossed beam experiments at room temperature for the O + CN reaction. This requires a full-dimensional study on the lowest ^{4}A″ state.[13]

Acknowledgment. Support from the Swedish Research Council is gratefully acknowledged. This study has been supported in part by the European Community's human potential Programme under Contract MCRTN 512302, Molecular Universe.

References and Notes

(1) Schulz, C.; Volpp, H.-R.; Wolfrum, J. In *Chemical Dynamics in Extreme Environments*; Dressler, R. A., Ed.; World Scientific Publishing: Singapore, 2001.
(2) Herbst, E.; Klemperer, W. *Astrophys. J.* **1973**, *185*, 505.
(3) Herbst, E.; Lee, H.-H.; Howe, D.; Millar, T. *Mon. Not. R. Astron. Soc.* **1994**, *268*, 335.
(4) Smith, I. W. M.; Herbst, E.; Chang, Q. *Mon. Not. R. Astron. Soc.* **2004**, *350*, 323.
(5) Boger, G. I.; Sternberg, A. *Astrophys. J.* **2005**, *632*, 302.
(6) Chapman, J. F.; Millar, T. J.; Wardle, M.; Burton, M. G. *Mon. Not. R. Astron. Soc.* **2009**, *394*, 394.
(7) Schmatjko, K. J.; Wolfrum, J. *J. Ber. Bunsen-Ges. Phys. Chem.* **1975**, *79*, 696.
(8) Schmatjko, K. J.; Wolfrum, J. *J. Ber. Bunsen-Ges. Phys. Chem.* **1978**, *82*, 419.
(9) Abrahamsson, E.; Andersson, S.; Nyman, G.; Marković, N. *Chem. Phys.* **2006**, *324*, 507.
(10) Prasad, R. *J. Chem. Phys.* **2004**, *120*, 10089.
(11) Schuurman, M. S.; Muir, S. R.; Allen, W. D.; Schaefer, H. F., III *J. Chem. Phys.* **2004**, *120*, 11586.
(12) Andersson, S.; Marković, N.; Nyman, G. *J. Phys. Chem.* **2003**, *107*, 5439.
(13) Abrahamsson, E.; Andersson, S.; Marković, N.; Nyman, G. *Phys. Chem. Chem. Phys.* **2008**, *10*, 4400.
(14) Andersson, K. et al. *MOLCAS version 5.2*; Lund University: Sweden, 2001.
(15) Yu, H. G.; Andersson, S.; Nyman, G. *Chem. Phys. Lett.* **2000**, *321*, 275.
(16) Yu, H. G.; Nyman, G. *J. Chem. Phys.* **2000**, *113*, 8936.
(17) Karlström, G.; Lindh, R.; Malmqvist, P.-Å.; Roos, B. O.; Ryde, U.; Veryazov, V.; Widmark, P.-O.; Cossi, M.; Schimmelpfennig, B.; Neogrady, P.; Seijo, L. *Comput. Mater. Sci.* **2003**, *28*, 222.
(18) Feit, M. D.; Fleck, J. A.; Steiger, A. *J. Comput. Phys.* **1982**, *47*, 412.
(19) Vibók, Á.; Balint-Kurti, G. G. *J. Phys. Chem.* **1992**, *96*, 8712.
(20) Marković, N.; Billing, G. D. *J. Chem. Phys.* **1994**, *100*, 1085.
(21) Stine, J.; Muckerman, J. *J. Chem. Phys.* **1976**, *65*, 3975.
(22) Everhart, E. In *Dynamics of Comets: Their Origin and Evolution*; Carusi, A., Valsecchi, G. B., Eds.; Reidel: Dordrecht, 1985.
(23) Bolton, K.; Nordholm, S. *J. Comput. Phys* **1994**, *113*, 320.
(24) Stine, J.; Muckerman, J. *J. Chem. Phys.* **1978**, *68*, 185.
(25) Preston, R.; Tully, J. *J. Chem. Phys.* **1971**, *54*, 4297.
(26) Schlier, C.; Nowotny, U.; Teloy, E. *Chem. Phys.* **1987**, *111*, 401.
(27) Andersson, S.; Marković, N.; Nyman, G. *Chem. Phys.* **2000**, *259*, 99.

JP904954K